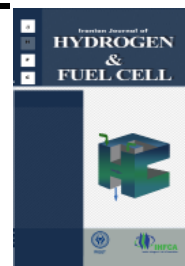


Iranian Journal of Hydrogen & Fuel Cell

IJHFC

Journal homepage://ijhfc.irostd.ir



Performance assessment of a SOFC cogeneration system for residential buildings located in eastern Iran

H. Hassanzadeh ^{1,*}, M. A. Farzad¹, A. Safavinejad¹, M. R. Agaebrahimi²

¹Department of Mechanical Engineering, University of Birjand, Birjand Iran

² Department of Electrical Engineering, University of Birjand, Birjand Iran

Article Information

Article History:

Received:

21 July 2016

Received in revised form:

25 Sep 2016

Accepted:

19 Oct 2016

Keywords

Solid Oxide Fuel Cell

Exergy

Optimization

CHP

Abstract

It is expected that residential units may replace traditional heat and power production systems with cogeneration ones. Among the different cogeneration systems, fuel cell based systems are a suitable choice due to their high efficiency, high power density, low emission and low noise. In this paper, a cogeneration system based on solid oxide fuel cells is examined. The system, including the fuel and air compressors, desulphurizer, fuel reformer, fuel cell stack, etc., has been modeled from an energy and exergy viewpoint. An optimization algorithm with three different objective functions, including power production, heat production and the minimum exergy destruction, is applied. Then, the base system is utilized along with photovoltaic and electrolyzer as a combined system. The results showed that an OP (Ordinary +Photovoltaic) is the best configuration with emissions reduction in the heat production approach, while OP and OFPE (Ordinary+Fuel cell+Photovoltaic+Electrolyzer) configurations are the best configurations with excess energy in power production approach. The conditions of the numerical calculations were selected in accordance with a sample building located in eastern Iran.

1. Introduction

Nowadays, more than 90% of consumed energy in the world is supplied by fossil fuels, most of which is consumed in transportation and power plants. In these units, the chemical energy of fuel is released during combustion, and less than 30% of the fuel chemical

energy is converted to mechanical energy while the rest is wasted. A substantial part of this wasted energy can be recycled by means of Combined Heat and Power (CHP) systems. In Iran, nearly 37% of total consumed energy and 52% of total electrical energy is consumed in residential, public and commercial sections [1]. The 30-35% efficiency of traditional residential systems can be improved to

*Corresponding Author's Fax: 06532202133
E-mail address: h.hassanzadeh@birjand.ac.ir

80% efficiency by means of cogeneration systems [2]. Therefore, substantial economic savings can be achieved by using cogeneration systems. Cogeneration systems can be used in any scale, if they match the heat demands. The selection of appropriate technology of CHP system is dependent on various subjects, such as the needed capacity, the operation cycle, space limitations, heat demands, environmental impact, available fuel, the costs of the grid, and the costs of connecting to the system. Major technologies in the cogeneration field are combustion engines, steam turbines, gas turbines, micro turbines and fuel cells. Among these technologies, fuel cells are receiving attention as an attractive choice due to their high efficiency and low emission. However, because this technology is not yet completely commercialized their installation costs are still high. Nevertheless, due to the low emissions generated in fuel cell systems they are very attractive in low capacity applications such as the residential sector. Fuel cells are electrochemical devices that convert the chemical energy of fuels directly to electrical energy without the limitations of the Carnot cycle [3, 4]. There are several types of fuel cells which are usually classified by their use of different electrolytes. Among them, solid oxide fuel cells (SOFC) have a substantial cogeneration potential due to their high operating temperature (600-1000 °C) and their ability to use natural gas directly. The schematic of a solid oxide fuel cell is shown in Fig. 1. This figure shows the partial oxidation fuel and air input to the anode and cathode channels of the fuel cell, respectively, followed by the H_2 and O_2 diffusing in the porous structure of electrodes and then reaching the electrode-electrolyte interface. O_2 molecules in the cathode catalyst are reduced by means of electrons and are converted to the oxide ion. These ions then pass through the solid electrolyte and react with H_2 molecules in the anode catalyst. During this reaction, the released electrons are transported to the cathode through an external circuit and the circuit is completed.

Several papers from different points of view and for different application of SOFC systems have been

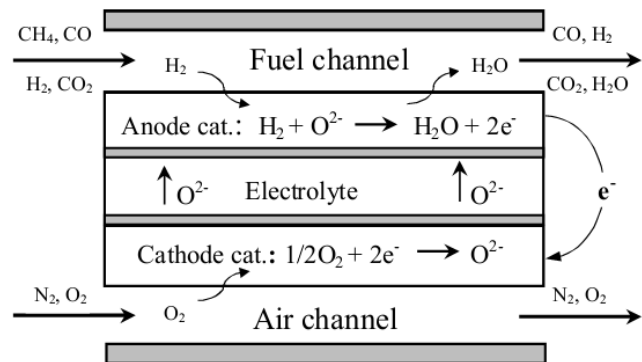


Fig. 1. Schematic of mass and charge transfer in SOFC.

published during the last decade. Rosen and Scott [5] compared various fuel cells from an energy and exergy efficiency viewpoint. They mentioned that increasing operation temperature increases energy and exergy efficiency and cogeneration potential. Hussain et al. [6] modeled a hydrogen SOFC system with an exergy approach. They showed that most exergy destruction occurs in the catalytic burner, and by using the waste heat in the catalytic burner to preheat fuel and air, exergy destruction is decreased. Rohani and Najafi [7] surveyed the composition of a SOFC and a gas turbine with an exergy approach. This work showed that the burner has the most exergy destruction. Lee and Strand [8, 9, 10] analyzed a natural gas SOFC system with an internal reformer for building applications. They developed a thermal and electrochemical model for a SOFC cogeneration system, and parametric analysis was carried out to investigate the effects of input flow rate, pre-reforming extent, fuel utilization and single cell voltage on produced power and electrical efficiency. Also, they compared various system configurations, such as a system without recycling, anode gas recycling, cathode gas recycling, and a combination of anode and cathode recycling and concluded that the last configuration was the best with considering produced power and efficiency analysis. In addition, this optimization study was carried out on an SOFC system for small and large-scale buildings under both hot and cold weather conditions. The optimization results varied widely

depending on system configurations and loading conditions. Bompard et al. [11] studied a 5kW SOFC power system for residential use from an economic point of view.

San et al. [12] presented a model for a power system based on tubular SOFCs for marine applications and validated the results with a 5 kW system from Siemens. Lamas et al. [13] studied a residential heat and power cogeneration system using an SOFC for a four person residence in Japan. The fuel considered for the system was a mixture of CH_4 and H_2 , adjusting the concentration ratio in order to improve heat output and lower CO_2 emissions. Hosseini et al. [14] analyzed a hybrid solar-fuel cell combined heat and power system from an energy and exergy point of view. The residential solar PV-electrolyzer system was coupled with a high temperature SOFC system for remote combined heat and power applications. In their analysis, they used the solar irradiance data published by the University of Toronto.

As can be seen, the specification of CHP systems in different areas depends on the region's climate, the potential of renewable energy, the availability of the energy carrier, environmental restrictions and so on. Therefore, continuing research in different areas is necessary. Accordingly, the main goal of this paper is representing a mathematical model for the analysis of a residential cogeneration system

based on a solid oxide fuel cell. For this purpose, the validated model of a single solid oxide fuel cell with internal reforming is used in a cogeneration system [15] and the energy and exergy efficiencies are examined. Then, the CHP system is incorporated into a combined system along with a photovoltaic and electrolyzer system to supply heat and power demands of a sample building in the eastern region of Iran. Furthermore, the various configurations are introduced and their efficiencies and emissions are compared.

2. Modeling

The schematic of a fuel cell system and its components are shown in Fig. 2. The solid and dashed lines present fluid and power flows, respectively. In this system, natural gas enters the compressor until the working pressure of system is attained. Then, it passes through a desulfurizing element to remove the sulfur contents. In the ejector, free sulfur gas is mixed with steam and then enters the pre-reformer. Gas exhausted from the pre-reformer passes through the mixing valve and enters the fuel cell stack. Beside the natural gas, generated hydrogen via water electrolysis from the photovoltaic system can be stored and used to generate electricity in a fuel cell stack when required. In order to prevent thermal stress, hydrogen leaving the tank enters the heater to be heated to the same temperature as the gas

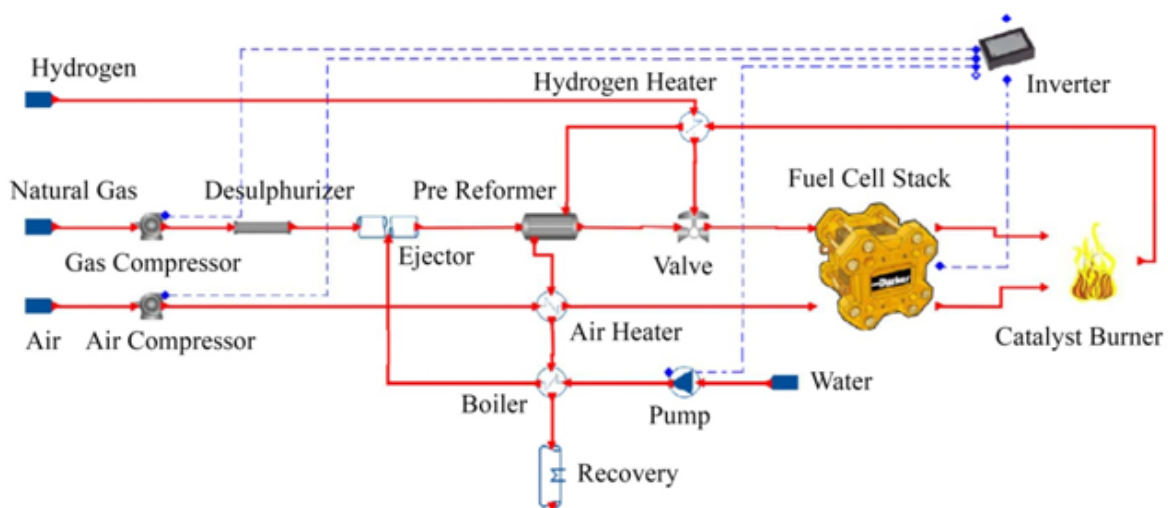


Fig. 2. Cogeneration system schematic without anode and cathode recycling. The solid and dashed lines present fluid and power flows, respectively.

leaving the pre-reformer, then the hydrogen enters the valve and these two streams are mixed with each other. As another input, air is compressed in the air compressor, and after being heated, enters the cathode channel of the fuel cell stack. The existing flow from the fuel cell stack enters the catalytic burner and the hot gas is used in the hydrogen heater, pre-reformer, air heater, boiler and heat recovery, respectively. The generated electrical power of the fuel cell stack is DC and must be converted to AC. The inverter performs this task. A part of the generated power is consumed in the system and the remaining power leaves the system as net power.

2.1. System Components

In this section different parts of the system are introduced and a brief explanation about modeling of each part is presented. For brevity, only some of the main equations are given and the rest are referenced.

2.1.1. Supply Terminals

Assuming that fuel, air, hydrogen and water streams are supplied from big reservoirs, the temperature, pressure, and properties of input streams are considered constant.

2.1.2. Compressor and Pump

The temperature of the exhaust gas increases during compression in the compressor. In an adiabatic reversible process, the exit temperature of the compressor can be calculated from an isentropic equation [16]. Using the isentropic efficiency and ideal gas assumption, the actual amount of temperature rise in the compressor can be calculated. Here, isentropic efficiency for the gas and air compressors is achieved from a screw compressor made by Lysholm Corporation [17]. If we ignore the mixing and reaction in turbo machines, species conservation law is valid and the momentum conservation law can be simplified to flow pressure rise.

2.1.3. Desulphurizer

Due to the sensitivity of solid oxide fuel cells to sulfur, desulfurizing is essential. In general, maximum sulfur content for preventing power loss is less than 0.1 ppm [18], but the acceptable range is 1-10 ppm [19]. In small residential applications, using a zinc oxide bed reactor is commercially attractive. It is assumed that this element is adiabatic and has 100 mbar pressure losses [19].

2.1.4. Ejector

An ejector is used to inject steam to the incoming natural gas. The ejector is a simple pump that has no moving parts. The operating concept of the ejector (or jet pump) is to use a high-pressure gas stream to entrain gas flow at a lower pressure by momentum transfer [19]. The governing equations were derived based on adiabatic and fully developed flow assumptions. These equations depend on ejector geometry, so expansion ratio and input diameter are the working parameters. Another working parameter is the steam to carbon ratio which is defined as the ratio of molar flow rate of water to the sum of molar flow rates of methane and carbon monoxide. The suction side flow rate is also defined by this parameter.

2.1.5. Pre-reformer

By adding steam to the fuel at a specific temperature, we can produce a hydrogen-rich mixture. Depending on the working situation, the heat demand of steam reforming reaction can consume 40-70% of produced heat in a fuel cell, and so the cooling method can be simplified to change excess air [20]. Thus, fuel cells with internal reforming have higher overall efficiency and less cost and complexity compared to low temperature fuel cells [18]. A pre-reformer is essential in a solid oxide fuel cell system with internal reforming. Preheating the supplied fuel to the fuel cell, reforming heavier hydrocarbons and preventing carbon deposition are the reasons for

this necessity. Generally, a pre-reformer is a heat exchanger with a catalyst bed through which the fuel mixture is passed, the tube and heating stream is passed through the shell. The pre-reforming reaction can include steam reforming, partial oxidation and auto-thermal reforming, but steam reforming is more common. Therefore, the needed heat supply is achieved from the exit stream of the catalytic burner. In some situations, this structure is made as a part of a catalytic burner. The species that enter the tube side react based on the steam reforming reaction ($\text{CH}_4 + \text{H}_2\text{O} \rightarrow \text{CO} + 3\text{H}_2$) and water-gas shift reaction ($\text{CO} + \text{H}_2\text{O} \rightarrow \text{H}_2 + \text{CO}_2$). Species that enter the shell side exit without any reaction. It is assumed that the element is adiabatic and tube and shell pressure losses are 50 mbar and 25 mbar, respectively [19].

2.1.6. Mixing Valve

When hydrogen is commercially available, it can be injected into the system. This situation occurs when a low price power supply for producing hydrogen is available, such as renewable energies. Mixing hydrogen with the fuel stream is the job of the mixing valve. It is assumed that this element is adiabatic and exit pressure is calculated from mass conservation and ideal gas laws.

2.1.7. Fuel Cell Stack

By ignoring the pressure loss in junctions and distributor channels, the behavior of a single fuel cell can be extended to a stack [21, 22]. This single cell is modeled based on mass, momentum and energy conservation laws [22]. Fuel cell stack working parameters are fuel utilization, excess air, average current density and the number of cells in the stack. It is assumed that the heat transfer occurs in the mean temperature of the fuel cell stack.

2.1.8. Catalytic Burner

Not all entered fuel in the fuel cell is consumed and some exits with anode leaving gases. Entering

air is also more than needed and large amounts of high temperature oxygen exist in cathode output. Using this air and fuel is essential to prevent energy waste in fuel cell systems. For this reason using a burner, an ordinary burner or a catalytic burner, in the downstream is common. Using a catalytic burner can decrease noise, and due to the absence of extreme mixing and combustion irreversibility is decreased and efficiency is improved. A well designed catalytic burner can recover 35-55% LHV of entered fuel as heat [23]. Because the cathode output flow rate is more than required, it is assumed that all fuel (methane, hydrogen and carbon monoxide) is completely oxidized. Due to lack of data about the geometry of this element, it is assumed that this element is adiabatic and has 20 mbar pressure losses [19].

2.1.9. Heat Exchanger

A heat exchanger is an essential part of cogeneration systems. This can be gas-gas for air or fuel preheating or a fuel reformer or gas-liquid to produce steam for the fuel reformer [18]. By using a pre-reformer, entered fuel does not require preheating but entering air must be heated to 500°C. Because there is no reaction in heat exchangers, the species composition can be considered constant. Due to little information about the heat exchanger for fuel cells, it is assumed that it is adiabatic and has 100 mbar pressure losses in each side [19].

2.1.10. Heat Recovery

Actually, recovery is a heat exchanger which is used for producing heat for external demands.

2.1.11. Inverter

The inverter is a device which converts DC current to AC. The efficiency of the inverter is in the range of 87-94%. This parameter is a function of inverter type and the load value. It is assumed that the inverter efficiency is 90% independent of the load [19].

2.2 System operation characteristics

Operation characteristics are used to compare the operating system in various situations. The operation characteristics of the selected system are net power, net heat, irreversibility and the efficiencies of first and second laws of thermodynamic for power, heat and cogeneration, which are described here. AC electrical power output from the inverter is defined as net electric power and the heat recovered in recovery is defined as net thermal power output. Irreversibility rate in the system is described based on the exergy balance as follows:

$$\begin{aligned} \dot{i} = & \left(1 - \frac{T_0}{T_{GC}}\right) \dot{Q}_{GC} + \left(1 - \frac{T_0}{T_{AC}}\right) \dot{Q}_{AC} + \left(1 - \frac{T_0}{T_P}\right) \dot{Q}_P \\ & + \left(1 - \frac{T_0}{T_{FC}}\right) \dot{Q}_{FC} + \left(1 - \frac{T_0}{T_R}\right) \dot{Q}_R + \left(1 - \frac{T_0}{T_I}\right) \dot{Q}_I \\ & - \dot{W}_{net} + \sum_{input} \dot{n}_i \psi_i - \sum_{output} \dot{n}_i \psi_i \end{aligned} \quad (1)$$

where GC, AC, P, FC, R and I indicate gas compressor, air compressor, pump, fuel cell stack, recovery and inverter, respectively [5]. Input and output exergy of the system are calculated from the air compressor, gas compressor, pump, hydrogen heater input and recovery accessories. Power and heat efficiencies are also defined as follows:

$$\mathcal{E}_{el}^I = \frac{\dot{W}_{net}}{\dot{n}_{fuel} LHV_{fuel}} \quad (2)$$

$$\mathcal{E}_{el}^I = \frac{\dot{W}_{net}}{\dot{n}_{fuel} LHV_{fuel}} \quad \mathcal{E}_{co}^{II} = \frac{\dot{W}_{net}}{\dot{n}_{Fuel} \psi_{Fuel} + \dot{n}_{Air} \psi_{Air} + \dot{n}_{Water} \psi_{Water}} \quad (3)$$

$$\mathcal{E}_{he}^I = \frac{\dot{Q}_R}{\dot{n}_{fuel} LHV_{fuel}} \quad (4)$$

$$\mathcal{E}_{he}^{II} = \frac{\dot{Q}_R \left(1 - \frac{T_0}{T}\right)}{\dot{n}_{Fuel} \psi_{Fuel} + \dot{n}_{Air} \psi_{Air} + \dot{n}_{Water} \psi_{Water}} \quad (5)$$

where T_0 is surrounding temperature and T is the temperature in recovery. Cogeneration efficiency, as

the sum of heat and power efficiencies is defined as follows:

$$\mathcal{E}_{co}^I = \frac{\dot{W}_{net} + \dot{Q}_R}{\dot{n}_{fuel} LHV_{fuel}} \quad (6)$$

$$\mathcal{E}_{co}^{II} = \frac{\dot{W}_{net} + \dot{Q}_R \left(1 - \frac{T_0}{T}\right)}{\dot{n}_{Fuel} \psi_{Fuel} + \dot{n}_{Air} \psi_{Air} + \dot{n}_{Water} \psi_{Water}} \quad (7)$$

3. System analysis and results

The mathematical equations are solved in steady state by gPROMS Model Builder 3.4.0. This software uses the LU factorization algorithm for solving linear algebraic equations, Newton method for nonlinear algebraic equations, Runge-Kutta and finite difference algorithms for algebraic-differential equations, and simple and multiple shooting for optimizations problems [24-26].

This system has 19 working parameters which must be calculated. It is assumed that the system works at the fuel cell maximum power and hydrogen heater output temperature is equal to pre-reformer output temperature. Initially, the system was modeled using reference working parameters shown in Table 1.

The pressure and temperature flow diagram is shown in Fig. 3. As can be seen, the greatest pressure loss occurred in the fuel cell air channel and the greatest temperature change occurred in the catalytic burner. The system flow exergy diagram is shown in Fig. 4. As shown in this figure, 141.083 kW, 0.225 kW and 0.30 kW exergy enters the system by fuel, air and water streams, respectively, and 1.189 kW exergy exits the system from recovery. The greatest exergy change (56.5kW) occurred in the anode channel of the fuel cell.

A work, heat and irreversibility diagram of the system is shown in Fig. 5. In this figure W , Q , QQ

Table 1. System's Working Parameters

Working parameter	Value	Comments
Pressure increase in gas compressor, $\Delta P_{\text{Gas compressor}}$	2.2 bar	Based on atmospheric pressure at recovery outlet and maximum 0.1 bar pressure difference in fuel cell stack inlets
Pressure ratio at gas compressor maximum efficiency working point	3.2	Base situation assumption
Flow rate at gas compressor maximum efficiency working point	0.170 mol/s	Base situation assumption
Pressure increase in air compressor, $\Delta P_{\text{Air compressor}}$	0.67 bar	Based on atmospheric pressure at recovery outlet and maximum 0.1 bar pressure difference in fuel cell stack inlets
Pressure ratio at air compressor maximum efficiency working point	1.67	Base situation assumption
Flow rate at air compressor maximum efficiency working point	2.101 mol/s	Base situation assumption
Pressure increase in pump, ΔP_{Pump}	0.1 bar	Based on atmospheric pressure at ejector suction inlet
Pre-reformer tube outlet temperature, $T_{\text{Pre-Reformer}}^{\text{Tube-out}}$	1073 K	Base situation assumption
Air heater tube outlet temperature, $T_{\text{Air Heater}}^{\text{Tube-out}}$	1073 K	Base situation assumption
Boiler tube outlet temperature, $T_{\text{Boiler}}^{\text{Tube-out}}$	420 K	assumption
Recovery shell outlet temperature, $T_{\text{Recovery}}^{\text{out}}$	353 K	assumption
Ejector expansion ratio, δ	2	assumption
Hydrogen mixing percent, X	0 %	assumption
Steam to carbon ratio, SC	2	Based on fuel cell working point
Fuel pre-reforming extent x	30 %	Based on fuel cell working point
Fuel cell stack fuel utilization, U_f	50 %	Based on fuel cell working point
Fuel cell stack excess air, λ_a	2.60	Based on fuel cell working point
Fuel cell stack average current density, \bar{j}	30,204 A/m ²	Based on fuel cell working point
Single cells in the fuel cell stack, n	1000	assumption

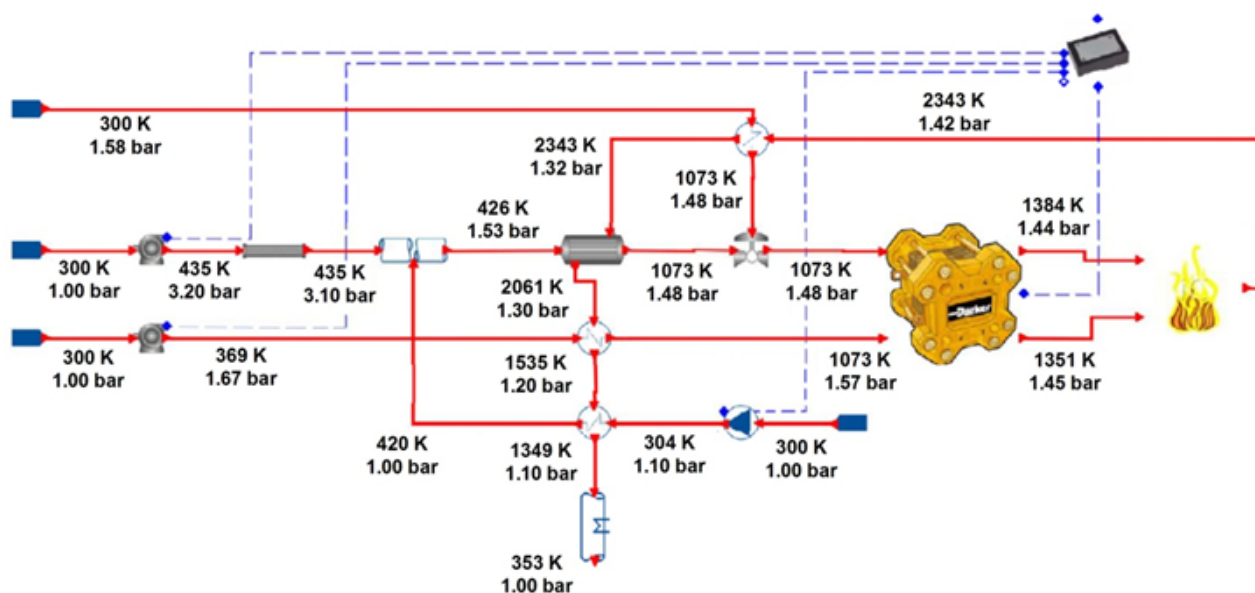


Fig. 3. System pressure and temperature flow diagram at base situation.

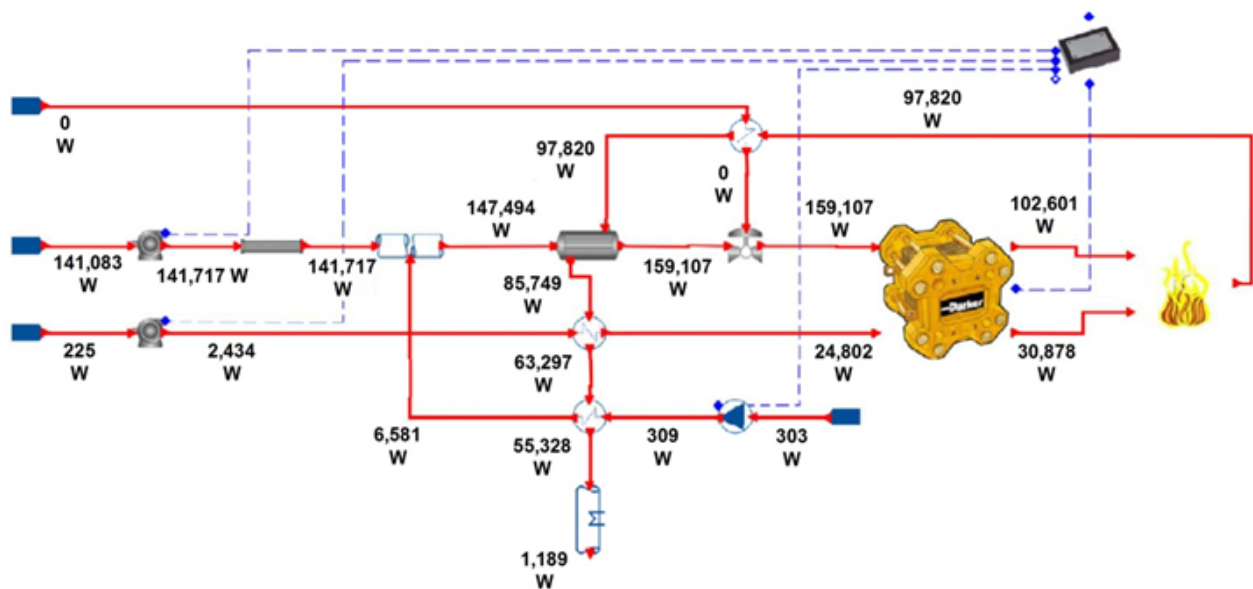


Fig. 4. System flow exergy flow diagram at base situation.

and I represent work, heat transfer to surrounding, internal heat transfer and irreversibility, respectively.

As shown in Fig. 6, the system net power is 27.68 kW and the air compressor is the main internal consumer. Also, the recovered heat is 115.23 kW and the wasted heat is 4.23 kW. To maintain the fuel cell stack at its working temperature, 2.42 kW heat is needed.

As shown in Fig. 7, nearly 95.52 kW exergy is wasted in different sections of the system, most

of which is due to the recovery and catalytic burner. The system efficiencies are also shown in Table 2.

3.1. System optimum working point

Working parameters are different depending on the system used for producing power or heat. In this section, the working point of the system for three approaches of power producing, heat producing and minimum exergy destruction

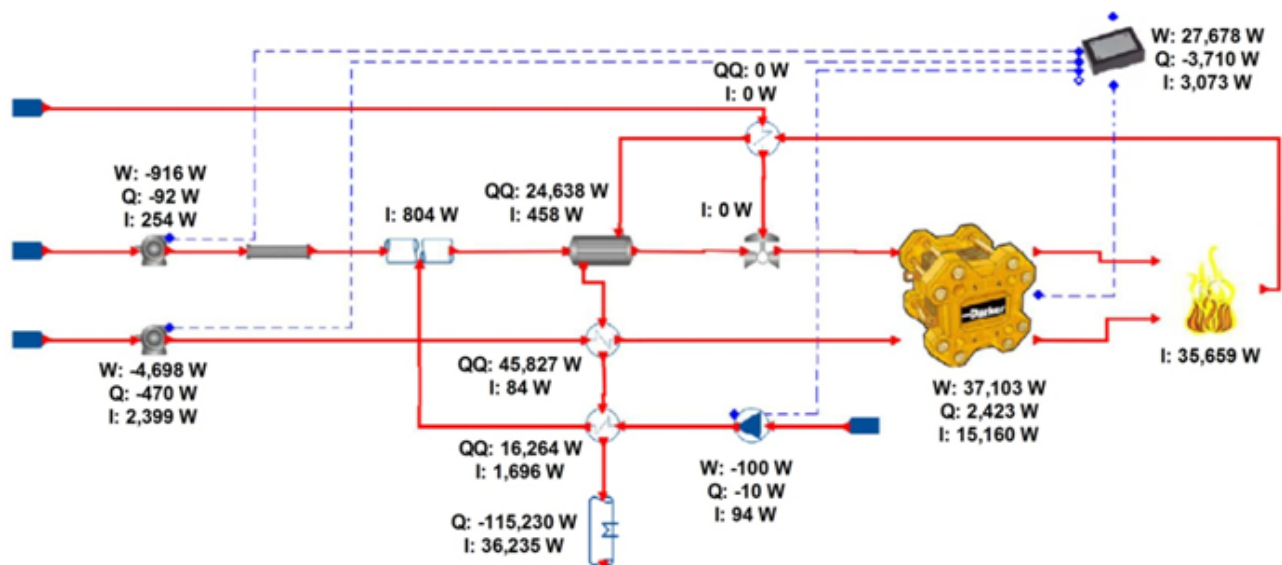


Fig. 5. System work, heat and irreversibility flow diagram at base situation.

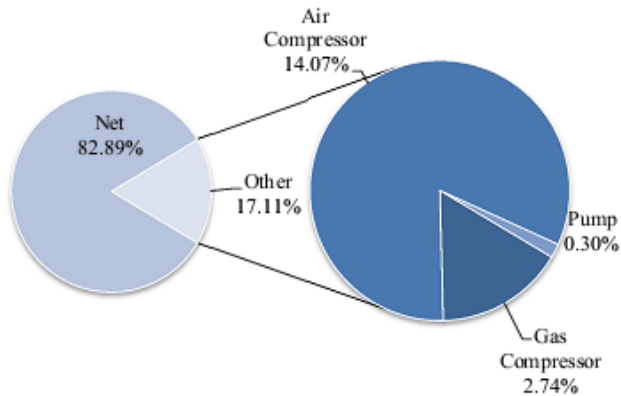


Fig. 6. Power balance in the system.

Table 2. The System Efficiencies

First law efficiency in power production	18.3%
Second law efficiency in power production	19.5%
First law efficiency in heat production	76.4%
Second law efficiency in heat production	12.6%
First law efficiency in cogeneration	94.7%
Second law efficiency in cogeneration	32.2%

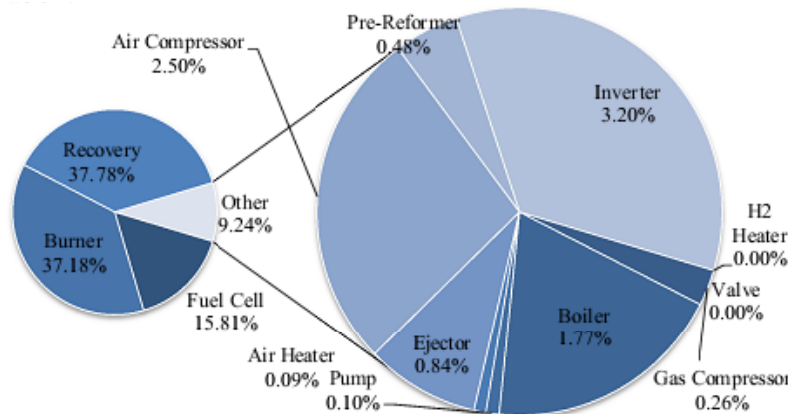


Fig. 7. Exergy destruction balance in system.

are determined. For this reason, three objective functions, shown in Table 3, are defined. The other parameters, not mentioned in this table, are constant and equal to the values in Table 1. Working parameters at the optimum point are shown in Table 4.

As shown in Table 4, less exergy is wasted in the power approach. This is due to the fact that more fuel is consumed in the fuel cell and less in the catalytic burner. Fuel utilization and fuel cell stack current density are the most important parameters in controlling exergy destruction, which also control the heat to power ratio of the system.

4. CHP Configuration

In this section, the auxiliary units are introduced and the environmental effects and energy balance of the system at different structures are discussed.

4.1. Auxiliary units

4.1.1. Consumer

The first auxiliary part is the consumer, which is a building with 10 apartments and a total of 900 m² area, located in Birjand, in the east of Iran. The type of materials used in the building reflects the traditional architecture and materials used in the construction of buildings in the city. A two-pipe fan coil system is used for heating and cooling. Hourly heating and cooling loads are calculated by HAP Software (Carrier). The building heating load is supplied by a central heating system and the cooling load is supplied by a lithium-bromide absorption chiller.

As shown in Fig. 6, the maximum and minimum heat demand for this consumer is 0.03 kW and 76.87 kW, respectively. These quantities are 1.20 kW and 10.20 kW, respectively, for the electrical demand.

Table 3. Conditions and Controls for finding System Optimum Working Points

Objective Function	
Power producing approach	MAX($\varepsilon_{el-AC}^I P$)
Heat producing approach	MAX($\varepsilon_{hc}^I Q$)
Minimum exergy destruction approach	MIN(\dot{i})
Controls	
Fuel cell stack average current density (A/m ²) [18]	2,000 < j < 35,000
Pre-reformer tube outlet temperature (K) [23]	823 < T _{Pre-Reformer} ^{Tube-out} < 1073
Air heater tube outlet temperature (K) [23]	823 < T _{Air Heater} ^{Tube-out} < 1073
Fuel cell stack fuel utilization (%) [19]	50 < U _f < 90
Fuel cell stack excess air [19]	2 < λ _a < 14
Fuel pre-reforming extent (%) [19]	5 < x < 30
Steam to carbon ratio [19]	2 < SC < 10
Pressure increase in gas compressor (bar)	0.01 < ΔP _{Gas compressor} < 5
Pressure increase in air compressor (bar)	0.01 < ΔP _{Air compressor} < 5
Pressure increase in pump (bar)	0.01 < ΔP _{Pump} < 5
Boiler tube outlet temperature (K)	373 < T _{Boiler} ^{Tube-out} < 450
Ejector expansion ratio [19]	1.5 < δ < 5
Conditions	
Fuel cell stack voltage (V) [19]	0.5 < V
Maximum temperature gradient in PEN [18]	$\left. \frac{dT_{PEN}}{dx} \right _{max} < 1000$
Pressure at anode inlet (bar)	1.3 < P _{Fuel Cell} ^{Anode inlet} < 5
Pressure at cathode inlet (bar)	1.3 < P _{Fuel Cell} ^{Cathode inlet} < 5
Pressure difference between anode and cathode (bar)	0 < P _{Fuel Cell} ^{Cathode inlet} - P _{Fuel Cell} ^{Anode inlet} < 0.1

This building needs 284.13 MWh heat and 29.61 MWh electricity, annually. As it can be seen, the heat to power ratio on the consumer side is extremely variable. When using a solid oxide fuel cell, which is very sensitive to load variation, control of the heat to power ratio on the producer side is vital.

4.1.2 Estimates of solar energy in the region

In the area under study, there are more than 280 days of sunshine per year and the solar energy potential is considerable. To estimate the solar energy potential, the data from the Center for Atmospheric scientific studies over a period of 22 years (2005-1983) were used for the city of Birjand. In Fig. 9 validation is done with the help of NASA data.

4.1.3. Photovoltaic Array

The power of the photovoltaic system is calculated

by the following equation [27]:

$$P = A_c G_T \eta_{mp,ref} \eta_e \left[1 + \frac{\mu_{mp}}{\eta_{mp,ref}} (T_a - T_{ref}) + \frac{\mu_{mp} G_T \tau \alpha}{\eta_{mp,ref} U_L} (1 - \eta_{mp,ref}) \right] \quad (8)$$

where A_c is the solar panel area, G_T is the solar radiation input, $\eta_{mp,ref}$ is the efficiency at maximum power in reference condition, η_e is the efficiency of power conditioner equipment, μ_{mp} is the thermal coefficient of efficiency at maximum power, T_a is the air temperature, and $T_{ref}=25K$ is the reference temperature.

$$\frac{\tau \alpha}{U_L} = (T_{c,NOCT} - T_{a,NOCT}) / G_{T,NOCT} \quad (9)$$

where $T_{c,NOCT}$, is the temperature of solar panels, $T_{a,NOCT}$ is the air temperature and $G_{T,NOCT}$ is the value of input radiation at working condition.

Table 4. Working Parameters of the System at Optimum Working Points

	Powerproducingapproach	Heatproducingapproach	Minimum exergy destruction approach
System working parameters			
Fuel cell stack average current density (A/m ²)	17,174	34,253	2,000
Pre-reformer tube outlet temperature (K)	1073	1073	823
Air heater tube outlet temperature (K)	1073	1073	1063
Fuel cell stack fuel utilization (%)	83.54	50	90
Fuel cell stack excess air	4.91	3.91	4.13
Fuel pre-reforming extent (%)	30.00	27.85	30.00
Steam to carbon ratio	3.07	4.58	2.00
Pressure increase in gas compressor (bar)	0.83	0.62	0.38
Pressure increase in air compressor (bar)	0.40	1.29	0.40
Pressure increase in pump (bar)	0.43	1.47	0.47
Boiler tube outlet temperature (K)	378	401	408
Ejector expansion ratio	4.57	2.01	2.02
System working characteristics			
Output power (kW)	16.24	16.52	2.84
Output Heat (kW)	25.34	143.14	1.83
Heat to power ratio	1.560	8.665	0.644
Exergy destruction (kW)	25.58	125.62	1.94
First law efficiency in power producing (%)	31.62	9.45	51.24
First law efficiency in heat producing (%)	49.35	81.89	32.94

Solar panels data are obtained from SUNTECH-STP 190-S [28]. Assuming that 60 m² is available on the roof and according to a yearly optimum slope angle of 25.4°, 50 panels can be installed on the roof. Therefore, the average photovoltaic power is 1.70 kW, which corresponds to 14.87 MWh in a year.

4.1.4. Electrolizer

The electrolizer is assumed to be a black box model [29], which obeys the following relationships:

$$I_0 = 0.0027 + 1.2450 P_0 - 0.4656 P_0^2 + 0.2206 P_0^3 \quad (10)$$

$$E = 3.2467 + 2.5499 I_0 - 1.7683 I_0^2 + 0.4178 I_0^3 \quad (11)$$

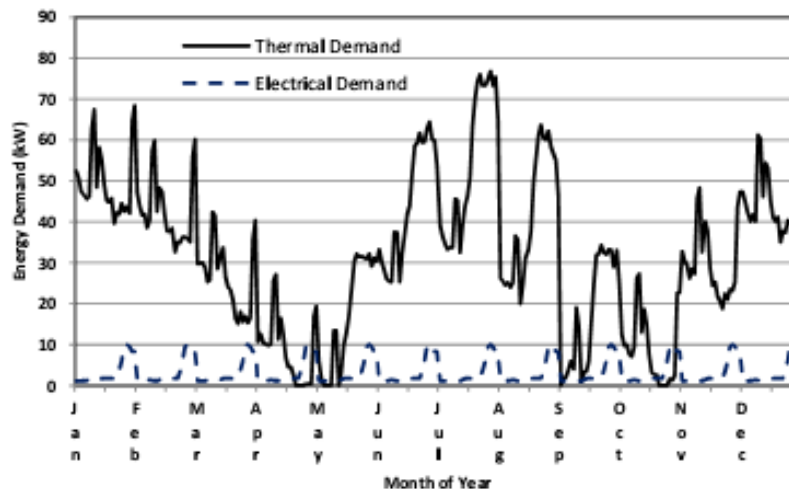


Fig. 8. Heat and power demand of the sample building.

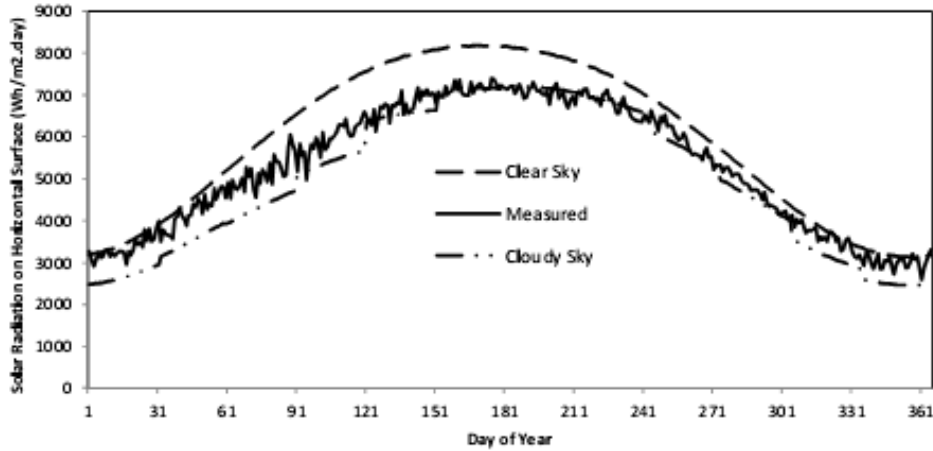


Fig. 9. Comparison of radiation measured and calculated according to data from NASA.

where E is the energy requested for producing 1 m^3 hydrogen in standard conditions and P_0 and I_0 are the normalized power and current of electrolyzer, respectively. The data are obtained from an ITM POWER -HBOX 30 polymer electrolyzer [30].

4.2. Emissions model

The emissions model used is based on the RET Screen program provided by the natural resources of Canada. This model can compare energy, operation costs and emissions of various configurations both in power and heat production schemes. The input data for this model are obtained from [1, 31].

4.2.1. Greenhouse gas emissions in power generation

The annual reduction of greenhouse gas emissions in power generation is calculated as follows:

$$\Delta_{\text{GHG,el}} = (e_{\text{base}} - e_{\text{prop}}) E_{\text{prop}} \quad (12)$$

where e_{base} and e_{prop} are greenhouse gas emissions in the base and proposed systems, respectively, and E_{prop} is the annual electricity consumption in the proposed system. Greenhouse gas emissions are calculated as follows in both the base and proposed system:

$$e = \left(e_{\text{CO}_2} \text{GWP}_{\text{CO}_2} + e_{\text{CH}_4} \text{GWP}_{\text{CH}_4} + e_{\text{N}_2\text{O}} \text{GWP}_{\text{N}_2\text{O}} \right) \frac{1}{\eta} \frac{1}{1-\lambda} \quad (13)$$

where e_i is the emission per produced power and GWP_i is the greenhouse potential of the specific gas. η and λ are the fuel conversion efficiency and losses in transfer and distribution lines, respectively.

4.2.1. Greenhouse gas emissions in heating and cooling

The governing equation for heating and cooling is as follows:

$$\Delta_{\text{GHG,hc}} = \left(\Delta_{\text{GHG,heat}} + \Delta_{\text{GHG,cool}} \right) \quad (14)$$

and the involving quantities are the same as described in the previous section, but in the heating or cooling process.

4.3. Configuration assessment

Here, various configurations are introduced and compared.

- Ordinary configuration (O): This is the usual configuration, in which heat demand is supplied by a gas fire boiler and the electricity is bought from the grid.
- Ordinary+Photovoltaic configuration (OP): This is the same as the base configuration, but part of the electrical demand is supplied from a photovoltaic system and the rest comes from the grid.
- Ordinary+Fuel cell configuration (OF): According to the fuel cell production strategy, some of the demand is supplied by a fuel cell and the rest is

produced similar to the ordinary configuration. In the power producing strategy, it is assumed that the fuel cell capacity matches the average electrical demand, which is 3.38 kW, so the heat capacity is 5.27 kW. On the other hand, in the heat producing strategy, fuel cell capacity must match the average heat demand, which is 32.44 kW. This means the fuel cell power capacity is 3.75 kW.

- Ordinary+Fuel cell+Photovoltaic configuration (OFP): This, in fact, is a combination of OP and OF configurations. In the power producing strategy, electrical and heat capacity of the system are 1.68 kW and 2.62 kW, respectively. Likewise, these quantities are 3.75 kW and 32.44 kW, respectively, in the heat producing strategy.

- Ordinary + Fuel cell + Photovoltaic + Electrolyzer configuration (OFPE): This configuration is similar to OF, but here the photovoltaic power is used completely in the electrolyzer. The annual hydrogen production average is 0.521 m³/h. Since using hydrogen changes the working point of the system, the new points are obtained again, as shown in Table 5. In this way, in the power producing strategy, the electrical and heat capacity of the system are 3.38 kW and 5.22 kW, respectively. Likewise, these quantities are 0.67 kW and 32.44 kW, respectively, in the heat producing strategy.

- Grid Independent Configuration (G): Although the advantages of the solid oxide fuel cells are lost in the grid independent configuration, the comparison of this configuration to others can be helpful. Here, it is assumed that the entire fuel system is hydrogen and the line pressure is so high that no hydrogen compressor is needed. The working point of the system must be determined again. The allowable limit of the working

parameters of the system are shown in Table 6 and the optimization results are shown in Table 7.

Generally, three plans can be considered for this system. The first, electrical demand of the building is supplied by a photovoltaic system and the excess power is used for hydrogen production. This hydrogen is then consumed in a fuel cell system with a heat production strategy to supply the heat demand of the building. In the second plan, a fuel cell system with a power production strategy supplies the whole electrical demand of the building. Likewise, a fuel cell system with a heat production strategy supplies the whole heat demand of the building in the third plan. It should be noted that in all three plans the capacity of the system is determined by the largest demand of the building. In the second and third plans the hydrogen required for the fuel cell system is provided by a photovoltaic system.

5. CHP Results

In this section, the results of the assessment of various configurations are presented. Tables 8 and 9 are for a grid-connected system and Table 10 is for an off-grid system. All values have been calculated on a one-year operation basis.

As shown, the maximum emission reduction occurs in the OFP structure in a heat production strategy. Another factor in optimum system determination is excess energy. This factor becomes important when using this excess energy is not possible. This excess energy can be sold back to the grid, used for hydrogen production or used for industrial processes. In this

Table 5. Working Parameters of the System at Optimum Working Points

	Power Producing Approach	Heat Producing Approach
Output power (kW)	16.83	3.25
Output heat (kW)	26.00	158.06
Heat to power ratio	0.119	48.634
Exergy destruction (kW)	19.79	125.60
First law efficiency in power producing (%)	31.85	1.90
First law efficiency in heat producing (%)	49.22	92.26

Table 6. Conditions and Controls for finding Optimum Working Points of Grid Independent System

Objective Function	
Power producing approach	$\text{MAX}(\varepsilon_{\text{el}}^{\text{I}} P_{\text{el-AC}})$
Heat producing approach	$\text{MAX}(\varepsilon_{\text{he}}^{\text{I}} Q)$
Controls	
Fuel cell stack average current density (A/m ²) [18]	$2,000 < j < 35,000$
Pre-reformer tube outlet temperature (K) [23]	$823 < T_{\text{Pre-Reformer}}^{\text{Tube-out}} < 1073$
Air heater tube outlet temperature (K) [23]	$823 < T_{\text{Air Heater}}^{\text{Tube-out}} < 1073$
Fuel cell stack fuel utilization (%) [19]	$50 < U_f < 90$
Fuel cell stack excess air [19]	$2 < \lambda_a < 14$
Hydrogen line pressure (bar)	$1 < P_{\text{H}_2} < 5$
Pressure increase in air compressor (bar)	$0.01 < \Delta P_{\text{Air compressor}} < 5$
Conditions	
Fuel cell stack voltage (V) [19]	$0.5 < V$
Maximum temperature gradient in PEN [18]	$\left. \frac{dT_{\text{PEN}}}{dx} \right _{\text{max}} < 1000$
Pressure at anode inlet (bar)	$1.3 < P_{\text{Fuel Cell}}^{\text{Anode inlet}} < 5$
Pressure at cathode inlet (bar)	$1.3 < P_{\text{Fuel Cell}}^{\text{Cathode inlet}} < 5$
Pressure difference between anode and cathode (bar)	$0 < P_{\text{Fuel Cell}}^{\text{Cathode inlet}} - P_{\text{Fuel Cell}}^{\text{Anode inlet}} < 0.1$

Table 7. Working Parameters of the Grid Independent System at Optimum Working Points

	Power producing approach	Heat producing approach
System working parameters		
Fuel cell stack average current density (A/m ²)	27,486	35,000
Pre-reformer tube outlet temperature (K)	1073	1073
Air heater tube outlet temperature (K)	1073	1073
Fuel cell stack fuel utilization (%)	77.72	50.00
Fuel cell stack excess air	4.76	8.30
Hydrogen line pressure (bar)	1.4	3.73
Pressure increase in air compressor (bar)	0.40	2.83
System working characteristics		
Output power (kW)	32.96	1.00
Output Heat (kW)	61.77	200.24
Heat to power ratio	1.87	200.24
Exergy destruction (kW)	50.41	150.00
First law efficiency in power producing (%)	28.46	0.44
First law efficiency in heat producing (%)	53.33	87.35

case, the OP configuration is optimum; however, when using a fuel cell, the OFPE in the power production configuration becomes optimum.

As can be seen, although the excess energy is minimum in the first plan, the shortage energy is maximum. If the goal is supplying the building

demands, the third plan is optimum.

Regardless of all of these factors, economic efficiency is the key factor. On this basis, according to the cost of energy and equipment, the OP configuration is the best structure for the studied sample.

Table 8. Characteristics of Various Combined Systems

Combined System	O	OP	OF (Power)	OF (Heat)
Photovoltaic Power Produced (MWh)	0.00	14.87	0.00	0.00
Fuel Cell Power Produced (MWh)	0.00	0.00	29.61	37.85
Fuel Cell Heat Produced (MWh)	0.00	0.00	46.17	284.17
Power from Grid (MWh)	29.61	23.29	11.73	10.84
Heat from Boiler (MWh)	284.13	284.13	242.01	68.37
Excess Power (MWh)	0.00	8.54	11.73	14.08
Excess Heat (MWh)	0.00	0.00	4.04	68.41
Hydrogen Produced (m ³)	0.00	0.00	0.00	0.00
CO ₂ Emission in Power Production (g/kWh)	0.00	0.00	563.48	1885.09
CO ₂ Emission in Heat Production (g/kWh)	0.00	0.00	361.08	217.61
Greenhouse Gas Emission in Power Production (kg/kWh)	2.33	1.83	2.71	22.99
Greenhouse Gas Emission in Power Production (kg/kWh)	13.75	13.75	11.83	3.57
Relative Greenhouse Gas Emission Reduction from Base System (kg)	---	15	534	2,279
Relative Greenhouse Gas Emission Reduction from Base System (%)	---	0.4	13.4	57.3

Table 9. Characteristics of Various Combined Systems (continued)

Combined System	OFP (Power)	OFP (Heat)	OFPE (Power)	OFPE (Heat)
Photovoltaic Power Produced (MWh)	14.87	14.87	0.00	0.00
Fuel Cell Power Produced (MWh)	14.72	32.85	29.61	5.87
Fuel Cell Heat Produced (MWh)	22.95	284.17	45.73	284.17
Power from Grid (MWh)	15.65	10.78	11.73	23.74
Heat from Boiler (MWh)	262.68	68.37	242.39	68.37
Excess Power (MWh)	15.62	28.88	11.73	0.00
Excess Heat (MWh)	1.50	68.41	3.99	68.41
Hydrogen Produced (m ³)	0.00	0.00	4,562.31	4,562.31
CO ₂ Emission in Power Production (g/kWh)	563.48	1885.09	487.86	8009.22
CO ₂ Emission in Heat Production (g/kWh)	361.08	217.61	315.65	185.51
Greenhouse Gas Emission in Power Production (kg/kWh)	2.12	22.98	2.46	95.87
Greenhouse Gas Emission in Power Production (kg/kWh)	12.77	3.57	11.83	3.51
Relative Greenhouse Gas Emission Reduction from Base System (kg)	284	2,283	541	140
Relative Greenhouse Gas Emission Reduction from Base System (%)	7.2	57.4	13.6	3.5

6. Conclusion

In this paper, a cogeneration system based on a solid oxide fuel cell was introduced for use in the eastern region of Iran. The performance of the fuel cell system was analyzed from first and second laws of thermodynamics viewpoints. Then, by means of optimization algorithms and defining three different objective functions, the operation of the system was optimized. The results show that the greatest variation of the flow exergy occurs in the fuel channel of the

fuel cell, the largest internal power consumer is the air compressor, and the maximum of irreversibility is made in the catalytic burner. Optimization results show that the power approach is more suitable than the others, because less exergy is wasted. In addition, various combined systems, such as OP (Ordinary + Photovoltaic), OFP (Ordinary + Fuel cell + Photovoltaic) and OFPE (Ordinary + Fuel cell + Photovoltaic + Electrolizer), were introduced and analyzed on energy and emissions bases. These comparisons show that the optimum configuration

Table 10. Characteristics of Various Combined Systems

Combined System	1 st Plan	2 nd Plan	3 rd Plan
Number of Solar Panels	82	265	650
Area for Solar Panels Installation (m ²)	95	306	750
Photovoltaic Power Produced (MWh)	13.5	0	0
Power Capacity of Fuel Cell (kW)	0.04	10.20	0.38
Heat Capacity of Fuel Cell (kW)	7.04	19.12	76.87
Hydrogen needed for Fuel Cell (mol/s)	0.0282	0.1255	0.3081
Fuel Cell Power Produced (MWh)	0.35	89.35	3.33
Fuel Cell Heat Produced (MWh)	61.67	167.49	673.38
Power Shortage (MWh)	22.69	0	26.28
Heat Shortage (MWh)	228.48	143.35	0
Excess Power (MWh)	0.14	59.74	0
Excess Heat (MWh)	6.02	26.71	389.25
Hydrogen Produced (m ³)	5,422	24,184	59,320
Number of Electrolizer	5	18	44

is the OFP in heat production according to the emissions, and OP and OFPE in power production according to the excess energy. The OFP plan is also the best for grid independent systems.

7. References

[1] Office, E.a.E.P., Energy Balance in 2009 and 2010, Energy Ministry: Tehran.

[2] Onovwiona H.I. and Ugursal V.I., "Residential cogeneration systems": review of the current technology. *Renewable and Sustainable Energy Reviews*, 2006, 10: 389.

[3] Hasanzadeh H. and Mansouri S.H., "Efficiency of ideal fuel cell and carnot cycle from a fundamental prospective". *Journal of Power and Energy*, 2005, 219: 245.

[4] Hassanzadeh H. and Farzad M.A., "Combined Fuel Cell and Photovoltaic System Assessment for CHP in House", 4th Fuel Cell Seminar, Tehran, Iran, 2010.

[5] Rosen M.A. and Scott D.S., "A Thermodynamic Investigation of the Potential for Cogeneration for Fuel Cells", *International Journal of Hydrogen Energy*, 1988,

13: 775.

[6] Hussain M.M., Dincer I., and Li X., "Energy and Exergy Analysis of an Integrated SOFC Power System", *CSME Forum*, 2004, 1.

[7] Rohani S. and Najafi A.F., "Thermodynamic Analysis of Solid Oxide Fuel Cell and Gas Turbine Combined Systems via Exergy", 25th International Power System Conference, Tehran, Iran, 2010.

[8] Lee K.H. and Strand R.K., "A System level Simulation Model of SOFC Systems for Building Applications", Third National Conference of IBPSA 2008, Berkeley, California, USA.

[9] Lee K.H. and Strand R.K. , "SOFC cogeneration system for building applications, part 1: Development of SOFC system-level model and the parametric study", *Renewable Energy*, 2009, 34: 2831.

[10] Lee K.H. and Strand R.K., "SOFC cogeneration system for building applications", part 2: System configuration and operating condition design, *Renewable Energy*, 2009, 34: 2839.

[11] Bompard E., Napoli R., Wan B. and Orsello G., "Economics evaluation of 5kW SOFC power system for

- residential use", *Int. Journal of hydrogen energy*, 2008, 33:3243.
- [12] San B.G., Zhou P.L. , and Clealand D., "Dynamic Modeling of Tubular SOFC for Marine Power System". *Journal of Marine Science and Application*, 2010, 9: 231.
- [13] Lamas H., Shimizu J., Matsumura E. and Senda J., "Fuel consumption analysis of a residential cogeneration system using a solid oxide fuel cell with regulation of heat to power ratio", *Int. Journal of Hydrogen Energy*, 2013, 38:16338.
- [14] Hosseini M., Dincer I. and Rosen M. A., "Hybrid solar-fuel cell combined heat and power systems for residential applications", *Energy and exergy analyses, J. Power Source*, 2013, 221: 372.
- [15] Farzad M.A. and Hassanzadeh H., "Modeling and optimization of a single planar solid oxide fuel cell", *Modares Mechanical Engineering*, 2015, 15: 81.
- [16] O'Hayre R.P., Cha Suk-Won, Colella W. and Printz Fritz B., "Fuel Cell Fundamentals", 2009, John Wiley & Sons.
- [17] Lysholm Corporation, 2012, Available from: www.lysholm.us.
- [18] Singhal, S.C. and Kendall K., "High Temperatures Solid Oxide Fuel Cells" *Fundamentals, Design and Application*, 2003: Elsevier.
- [19] Braun R. J., "Optimal design and operation of solid oxide fuel cell systems for small-scale stationary applications", 2002, PhD thesis, university of Wisconsin.
- [20] Aguiar, P., Adjiman C.S., and Brandon N.P., "Anode-supported intermediate temperature direct internal reforming solid oxide fuel cell. I: model-based steady-state performance. *Journal of Power Sources*, 2004, 138: 120.
- [21] Iora P., Aguiar P., Adjiman C.S., Brandon N.P., "Anode-supported intermediate temperature direct internal reforming solid oxide fuel cell. I: model-based steady-state performance. *Journal of Power Sources*, 2004, 138: 120.
- [21] Iora P., Aguiar P., Adjiman C.S., Brandon N.P., "Comparison two IT DIR-SOFC models": Impact of variable thermodynamic, physical, and flow properties. *Steady-state and dynamic analysis. Chemical Engineering Science*, 2005, 60: 2963.
- [22] Kang Ying-Wei, Li Jun , Cao Guang-Yi , Tu Heng-Yong , Li Jian , Yang Jie, "A reduced 1D dynamic model of a planar direct internal reforming solid oxide fuel cell for system research". *Journal of Power Sources*, 2009, 188: 170.
- [23] Aguiar, P., Adjiman C.S., and Brandon N.P., "Anode-supported intermediate-temperature direct internal reforming solid oxide fuel cell" II. Model-based dynamic performance and control. *Journal of Power Sources*, 2005, 147: 136.
- [24] "gPROMS Model Developer Guide", 2011, Process Systems Enterprise: London.
- [25] "gPROMS ModelBuilder Guide", 2011, Process Systems Enterprise: London.
- [26] "gPROMS Optimisation Guide", 2011, Process Systems Enterprise: London.
- [27] Duffie, J.A. and Beckman W.A., "Solar Engineering of Thermal Processes". 2nd Edition 1980: John Wiley & Sons.
- [28] Suntech Power Company. Available from: <http://www.suntech-power.com/>.
- [29] Bilgen, E., "Domestic hydrogen production using renewable energy". *Solar Energy*, 2004, 77: 47.
- [30] ITM Power Corporation. Available from: www.itm-power.com.
- [31] RETScreen, Natural Resources Canada.